

1 **Efficient low-temperature hydrogenation of fatty acids to fatty alcohols and alkanes**

2 **on a Ni-Re bimetallic catalyst: the crucial role of NiRe alloys**

3 Xincheng Cao ^a, Jiaping Zhao ^a, Feng Long ^a, Peng Liu ^a, Xia Jiang ^a, Xiaolei Zhang ^c, Junming Xu ^{a,b*},
4 Jianchun Jiang ^{a,b*}

5 ^a *Institute of Chemical Industry of Forest Products, Chinese Academy of Forestry; Key Lab. of Biomass*
6 *Energy and Material, Jiangsu Province; National Engineering Lab. for Biomass Chemical Utilization;*
7 *Key and Open Lab. on Forest Chemical Engineering, SFA, Nanjing 210042, China*

8 ^b *Co-Innovation Center of Efficient Processing and Utilization of Forest Resources, Nanjing Forestry*
9 *University*

10 ^c *Department of Chemical and Process Engineering, University of Strathclyde, UK*

11 * *Corresponding author: Tel. +86 2585482478; Fax: 025-85482485 E-mail: xujunming@icifp.cn, bio-energy@163.com.*

13
14 **Abstract:** Selective hydrogenation of fatty acids is important for production of sustainable fuels and
15 valuable chemicals as well as for the utilization of natural oils and fats. Generally, high reaction
16 temperature (>200°C) is required due to the weak polarizability and low reactivity of the carbonyl group
17 of fatty acids. Here, we report an efficient catalytic system (Ni-Re/SBA-15 bimetallic catalyst) that
18 realizes the low-temperature conversion of fatty acids to corresponding alcohols (reaction temperature:
19 150 °C) and diesel-range alkanes (170 °C) with high yields, surpassing the catalytic performance rendered
20 by most of the catalytic systems reported so far. Detailed investigation into the nature of the catalyst
21 showed that the superior activity originated from the formation of NiRe alloy, which improved the
22 dispersion of metallic Ni, the H₂ activation ability and promoted the fatty acids/alcohols adsorption on
23 the catalyst surface at low temperatures. More importantly, due to its strong electrophilicity, the fatty
24 acids with highly electronegative carbonyl oxygen can be preferentially adsorbed on the catalyst surface
25 than the fatty alcohols, which leads fatty acids to be converted preferentially. In this way, high catalytic

26 efficiency and fatty alcohol selectivity can be obtained at a low temperature (150 °C). Further increasing
27 reaction temperature to 170 °C, the reactant can be hydrodeoxygenated to form diesel-range alkanes.
28 This developed NiRe/SBA-15 catalytic system highlights a great prospect for production of valuable
29 fatty alcohols and alkanes from the conversion of bioderived fatty acids under mild conditions.

30 **Keywords:** Selective hydrogenation; Low-temperature conversion; Ni-Re bimetallic catalyst; Fatty
31 alcohols

32 1. Introduction

33 Bio-feedstocks rich in fatty acids and triglycerides such as natural oils and fats are promising for
34 producing the liquid biofuels and valuable chemicals [1, 2]. Recent years, vegetable oils and waste
35 cooking oils are being used as a low-cost renewable resources to produce the diesel-range alkanes, known
36 as the second-generation biodiesel, or the fatty alcohols that are important compounds for plasticizer,
37 cosmetic and lubricant productions [3-5]. For the production of diesel-range alkanes or fatty alcohols,
38 currently, commercial metal sulfide (NiMoS₄ and CoMoS₄) [6, 7] or copper-chromite (CuO/CuCr₂O₄) [8]
39 catalysts have been developed and applied for the hydrogenation of natural oils. However, harsh reaction
40 conditions (200~400 °C and high H₂ pressure) and the introduction of toxic S or Cr elements greatly
41 limited their application [9, 10].

42 In order to develop a highly efficient and environmentally friendly catalyst for the selective
43 hydrogenation of component of natural oils, at present, researches are mainly focused on the precious
44 metal or their derived bimetallic catalysts [11-13]. For instance, Liu et al. [11] proposed that the synergy
45 between the Ir metal and partially reduced ReO_x can effectively promote the conversion of vegetable oils
46 to diesel-range alkanes at low temperature (180 °C). Although these catalysts exhibited high catalytic
47 activities for the hydrogenation of lipids and their model compounds, it would be desirable to find an

48 abundant and economic catalysts that can still work at a low reaction temperature and H₂ pressure. In
49 this respect, metallic Ni is a promising for the hydrogenation of natural oils. However, it exhibits weak
50 hydrogenation activity at low temperature and high C-C bond hydrogenolysis activity at high
51 temperatures, which result in a low product yield. To improve catalyst activity and suppress the
52 occurrence of the side reactions caused by the single metallic Ni, a feasible strategy is to construct Ni-
53 based alloy or intermetallic compound (IMC). Since the introduced second metal can provide geometric
54 and /or electronic modification to the metallic Ni [14, 15]. In prior works, NiIn IMC [16], NiCu [5, 17]
55 and NiFe alloys [18] have been reported and exhibited remarkably results for the synthesis of fatty
56 alcohols and alkanes from the conversion of fatty acids. Although these catalysts showed high target
57 product selectivity, high reaction temperatures (≥ 250 °C) are still required due to the decreasing catalytic
58 activity. Therefore, developing a catalyst system with high activity and product selectivity is highly
59 demand for the conversion of fatty acids.

60 Rhenium species (Re metal or ReO_x) have been widely employed in the conversion of biomass
61 oxygen-containing compounds due to its strong oxophilicity activity [19-21]. In particular, the
62 combination of Re species with noble metals (Pd, Ir or Ru) are efficient for the hydrogenation of fatty
63 acids due to the synergy between the noble metal (Pd, Ir or Ru) and partially reduced ReO_x species [11,
64 22, 23]. As compared to combination of Re species with noble metals, however, few researches on the
65 NiRe bimetallic catalysts for the hydrogenation of fatty acids, and their intrinsic activities are not
66 revealed. One important reason may be that the reduction of NiRe catalysts requires a high reduced
67 temperatures (>400 °C) owing to the reduction of NiO to metallic Ni, which results in the Re species
68 mainly existing in the form of metallic Re instead of ReO_x on the catalyst surface. Compared with the
69 partially reduced ReO_x species which are rich in unsaturated active sites (Re²⁺, Re³⁺, Re⁴⁺, Re⁶⁺), metallic

70 Re (Re^0) is difficult to be used as an effective active metal assistant to promote the conversion of reactant
71 under mild conditions due to its relatively low oxophilicity activity.

72 In this work, we reported that after reduction at high temperature (500 °C) in a H_2 flow, the NiRe
73 alloys formed on the surface of the bimetallic catalysts can efficiently catalyze fatty acids conversion
74 into fatty alcohols or diesel-range alkanes at low temperatures (150~170 °C). Compared with the
75 previously reported combination of noble metal and partially reduced ReO_x catalytic system, the
76 developed NiRe bimetallic catalysts not only show similar or even higher catalytic activity for the
77 hydrogenation of fatty acids, but also exhibit tunable selectivity towards fatty alcohol and diesel-range
78 alkane products. In order to promote the dispersion of metal active sites, mesoporous silica material of
79 SBA-15 was selected as catalyst support because of its high surface areas and good thermal stability [24-
80 26]. Detailed characterization (XRD, H_2 -TPR, XPS and CO-FTIR) were performed to probe catalyst
81 structure and possible electronic interaction between the Ni and Re in the bimetallic catalyst. In-situ
82 FTIR of octanoic acid and DFT calculations were conducted to elaborate its high catalyst activity at low
83 temperature and reveal the underlying structure-activity relationship. Additionally, the several crucial
84 parameters, such as the Ni/Re molar ratio, reaction temperature, H_2 pressure and catalyst stability, were
85 also investigated.

86 2. Experimental section

87 2.1 Chemicals

88 $\text{Ni}(\text{NO}_3)_2 \cdot 6\text{H}_2\text{O}$ (purity, 98.0%), NH_4ReO_4 (purity, 99.9%), $(\text{NH}_4)_6\text{Mo}_7\text{O}_{24} \cdot 4\text{H}_2\text{O}$ (purity, 99.5%),
89 $\text{Fe}(\text{NO}_3)_3 \cdot 9\text{H}_2\text{O}$ (purity, 98.5%) were purchased from Macklin (Shanghai, China). SBA-15 (BET surface
90 area, 550-600 m^2/g , pore size: 6-11 nm) were purchased from XFNANO (Jiangsu, China). All chemicals
91 were used without further purification.

92 2.2 Catalyst preparation

93 The supported Ni_xRe_y bimetallic catalysts with different molar ratio were synthesized by co-
94 impregnation method, where x and y refer to the molar ratio of the metal atom. Typically, a calculated
95 amounts of Ni(NO₃)₂·6H₂O and NH₄ReO₄ were added into the solution containing SBA-15 support.
96 After impregnation for 12 h, the obtained samples were dried at 80 °C for 10 h and then calcined at 400°C
97 for 5.0 h in air. The amount of Ni loading related to the support was fixed at 10 wt% while the Re loading
98 was varied. Detailed amounts of metal loading were displayed in [Table S1](#). As for the monometallic
99 catalysts of Ni₁ and Re₁, they have identical molar loadings with the Ni₁Re₁ catalyst. For comparison,
100 Ni₁Mo₁ and Ni₁Fe₁ catalysts with 10 wt% Ni loading relative to support were also prepared using above
101 the method. Prior to use, the calcined samples were reduced at 500 °C for 3.0 h.

102 2.3 Catalyst characterization

103 Hydrogenation temperature programmed reduction (H₂-TPR) was employed to study the
104 reducibility of catalysts. The dispersion of metal particles over the catalyst surface was observed and
105 measured by transmission electron microscope (TEM). X-ray diffraction (XRD) and high resolution
106 transmission electron microscope (HRTEM) were used to analyze the formed species on the catalysts.
107 The electronic interaction between metals was explored by XPS and in situ FTIR spectroscopy of CO
108 (CO-FTIR). The amounts of hydrogen adsorption and acidic sites were measured by hydrogenation (H₂-
109 TPD) and ammonia temperature programmed desorption (NH₃-TPD), respectively. The interaction
110 between the reactant and tested catalyst was studied by in situ FTIR spectroscopy of propionic acid (PA).
111 The measured information about the test procedure can be found in [Supporting Information](#).

112 2.4 Computational details

113 To understand why the Ni₁Re₁ bimetallic catalyst shows high catalytic activity for the hydrogenation

114 of fatty acids at a low temperature, the density functional theory (DFT) calculations were performed
115 using the Perdew-Burke-Ernzerbof (PBE) approximation and the projector augmented wave (PAW)
116 method in the Vienna Ab initio Simulation Package (VASP) [27]. $2 \times 2 \times 1$ Monkhorst-Pack grid and an
117 energy cutoff of 550 eV were used in our calculations [18]. The propionic acid (PA) was selected as a
118 simplified model of fatty acids. A four-layer slab with 64 atoms for Ni(111) was modeled, a slab with 52
119 atoms for Re(111) and a larger slab with 144 atoms for Re_3Ni (111) was used. The vacuum length was set
120 as 15 Å along the z direction. The upper two-layer atoms for all models in the cell were relaxed. The
121 adsorption energy (E_{ads}) was calculated using the following equation [28]:

$$122 \quad E_{\text{ads}} = E_{\text{total}} - E_{\text{surface}} - E_{\text{adsorbate}} \quad (1)$$

123 where E_{total} was the total energy after the adsorption, E_{surface} was the calculated energy of the clean catalyst
124 and $E_{\text{adsorbate}}$ was the energy of the gas-phase molecule.

125 **2.5 Catalytic reaction and product analysis**

126 The catalytic hydrogenation reaction was carried out in an autoclave reactor (50 mL). Typically, the
127 reactor was added into fatty acid (0.1 g), activated catalyst (0.02 g) and cyclohexane solvent (10 mL).
128 Then, the reactor was pressurized with hydrogen to 4.0 MPa after removing air inside. The reactions
129 were operated at a temperature range of 130-170 °C under a stirring rate of 1000 rpm. After the reaction,
130 the obtained liquid product was analyzed by gas chromatography (GC, Agilent 7890A/5975C) equipped
131 with a FID and an (30m × 0.25 mm × 0.25 μm) HP-5 capillary column. Internal standard (i.e., eicosane)
132 was used for quantitative analysis.

133 The conversions of substrates and selectivity of target product were calculated using the following
134 equations (2-3):

(2)

(3)

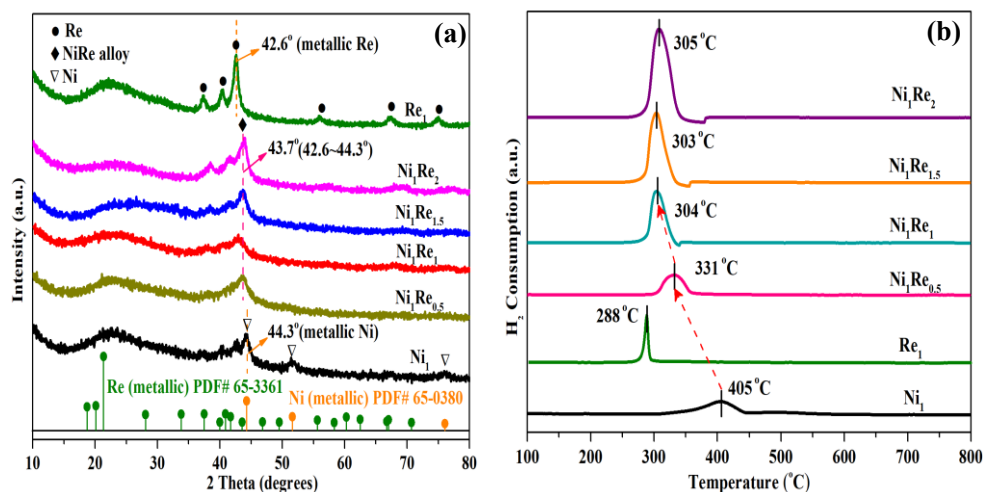
$$\text{Conversion} = \frac{\text{mol}_{\text{initial reactant}} - \text{mol}_{\text{unreacted reactant}}}{\text{mol}_{\text{initial reactant}}} \times 100\%$$

$$\text{Selec. (detec. products)} = \frac{\text{mol}_{\text{product}} \times n_{\text{C atoms in product}}}{\text{mol}_{\text{total C atoms in the liquid products detected}}} \times 100\%$$

3. Results and discussion

3.1 Catalyst characterization

The textural properties of the Ni_xRe_y/SBA-15 catalysts with different molar ratio of Ni/Re were analyzed by using N₂ adsorption-desorption, XRD, CO pulse adsorption, H₂-TPR and TEM. The N₂ adsorption-desorption isotherms of the catalysts were displayed in Figure S1 (a). All tested catalysts exhibited typical type VI isotherms with evident H1 hysteresis loop, indicating that the tested catalysts were typical mesoporous structure. Figure S1 (b) shows the corresponding pore size distribution curves and revealed that the pore sizes were centered at about 6-8 nm. The detailed textural parameters are listed in Table S2. Compared with the SBA-15 support without any metal loadings, the surface areas and total pore volume of the Ni_xRe_y/SBA-15 catalysts gradually decreased as the metal loading increased. In particular, when the Ni/Re < 1 (Ni₁Re_{1.5} and Ni₁Re₂), the surface area of the catalyst was drastically reduced, which could be attributed to the excessive Re metal loadings to form large metal particles, as indicated by the XRD results.

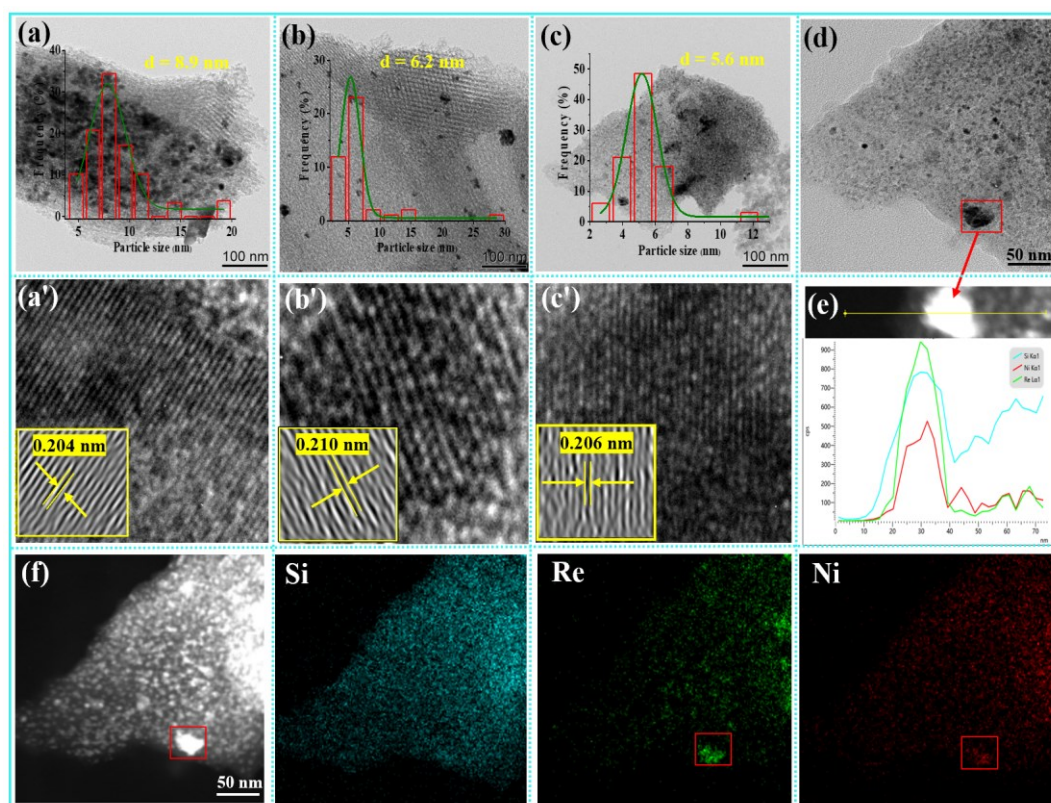


150

151 **Figure 1.** (a) XRD patterns of the reduced catalysts; (b) H₂-TPR profiles of the calcined catalysts.

152 XRD was performed to identify the phase composition of the catalysts. As shown in [Figure 1\(a\)](#),
153 after reduction at 500 °C for 3.0 h, the monometallic Ni₁ and Re₁ catalysts only showed the metallic Ni
154 and Re diffraction peaks, respectively, while the Ni_xRe_y bimetallic catalysts with different molar ratio
155 exhibited a different behavior from the Ni₁ and Re₁ catalysts. In the bimetallic Ni_xRe_y catalysts, for which
156 the introduction of Re component resulted in the lattice expansion of Ni unit cell, the diffraction peak
157 of Ni (111) at 2θ of 44.3° for monometallic Ni₁ shifted to a lower value of 43.7° for the Ni₁Re₁ catalyst.
158 This phenomenon reveals that the introduced Re component penetrated into the Ni lattice and formed
159 NiRe alloy. Moreover, no Ni species were detected in the bimetallic Ni_xRe_y catalysts, indicating that the
160 presence of Re favored the dispersion of Ni species. With the introduction of Re component, it was
161 observed that the Ni₁Re_{1.5} and Ni₁Re₂ catalysts displayed the diffraction peaks of metallic Re, which
162 results from the reduction of excess Re species to form large metal particles.

163 H₂-TPR was conducted to investigate the reducibility of catalysts and the interaction between metals
164 ([Figure 1\(b\)](#)). The Ni₁ and Re₁ only exhibited one hydrogen reduction peak at around 405 (Ni²⁺ to Ni⁰)
165 [29] and 288 °C (Reⁿ⁺ to Re⁰) [30], respectively. As for the Ni_xRe_y bimetallic catalysts, interestingly, it
166 was found that they also only showed one reduction peak at around 305 °C, in which the peak position
167 was located between Ni₁ and Re₁. This result suggests that the presence of Re promoted the reduction of
168 NiO (shifted from 405 to 305 °C) due to their strong interaction. Additionally, only one large hydrogen
169 reduction peak appeared in the bimetallic catalysts indicates that the introduced Ni and Re species may
170 form another compound of NiRe alloy during catalyst reduction process, as implied in the
171 characterization results of XRD and HRTEM ([Figure 2\(c'\)](#)).



172

173 **Figure 2.** TEM images of (a) Ni₁; (b) Re₁; (c and d) Ni₁Re₁; HRTEM image of (a') Ni₁; (b') Re₁; (c')
174 Ni₁Re₁; (e) EDS line spectra along the yellow line in e image; (f) HADDF-STEM image and elemental
175 mapping of Ni₁Re₁ catalyst.

176

In order to observe the dispersion of metal particles on the catalyst surface, TEM images were made.

177

As shown in [Figure 2\(a, b\)](#), the nickel particles on the surface of Ni₁ catalyst were obviously

178

agglomerated, while the Re₁ catalyst exhibited the uniform and small metal particles with average particle

179

sizes of 6.2 nm. These results indicate that Re species can be better dispersed on the SBA-15 support as

180

compared with the Ni species, which could be attributed to the strong oxophilicity of Re species [\[31\]](#). As

181

for the Ni₁Re₁ catalysts, it was found that the introduction of Re significantly reduced the metal particles

182

with the average size of 5.6 nm ([Figure 2\(c, d\)](#)), indicating that the added Re promoted the dispersion of

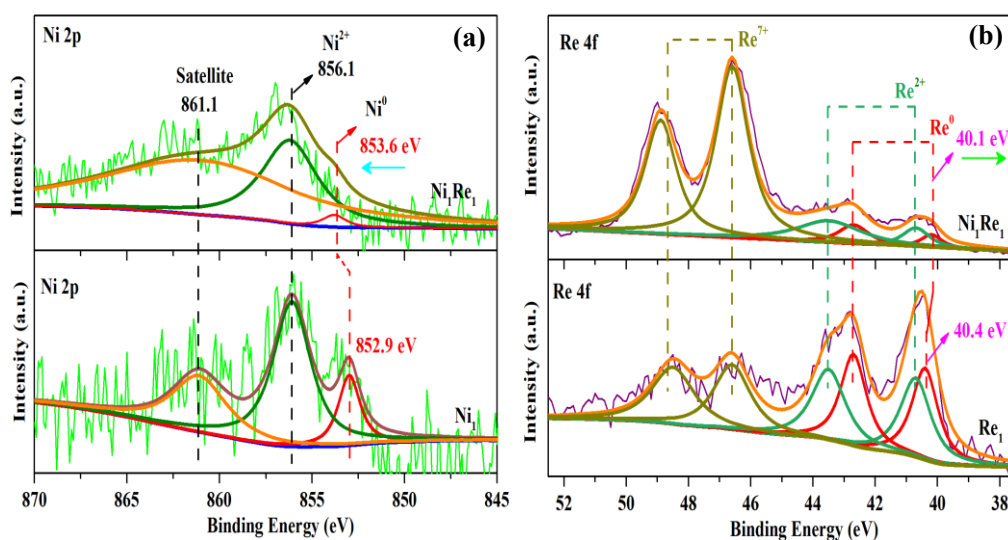
183

Ni species, in accordance with the XRD results. To further confirm this phenomenon, CO pulse

184

adsorption was performed to calculate the dispersion of metallic Ni ([Table S2](#)). After introducing the Re

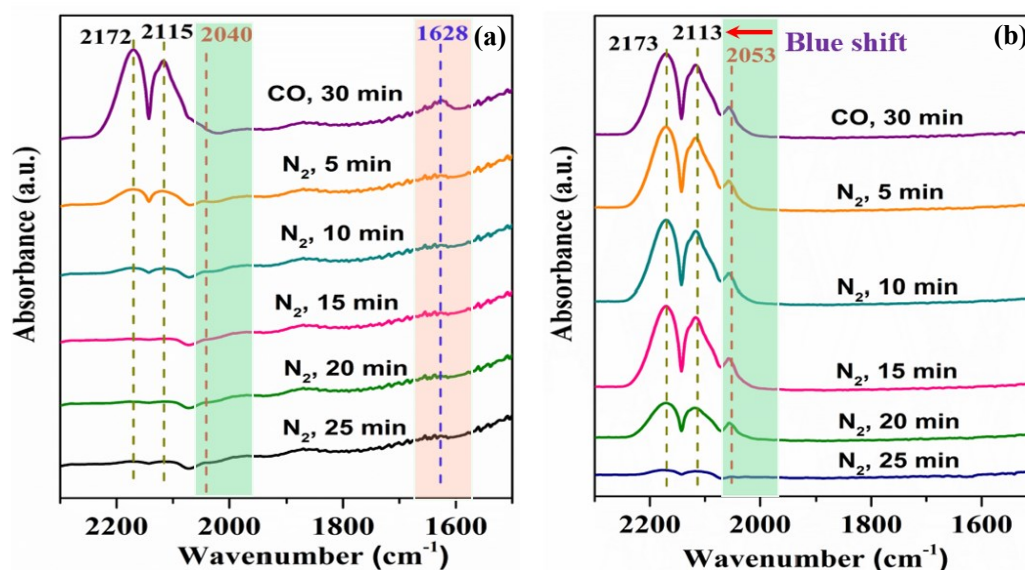
185 species, the dispersion of metallic Ni was improved from 1.8% of the Ni₁ to 3.2% of the Ni₁Re₁ catalyst.
186 According to the characteristic results (XRD, H₂-TPR, XPS and CO-FTIR), the promotional effect of Re
187 on the dispersion of the metallic Ni was attributed to the interaction between the Ni and Re.
188 HRTEM measurements were performed to identify the formed species on the surface of support.
189 For the Ni₁ and Re₁ catalysts, the lattice fringes of 0.204 and 0.21 nm were measured (Figure 2(a', b')),
190 corresponding to the Ni (111) and Re (101) spacings, respectively. As for the Ni₁Re₁ catalyst, the lattice
191 fringe of 0.206 nm was measured (Figure 2(c')), which was ascribed to the NiRe alloy [31]. In good
192 agreement with the XRD and H₂-TPR results, these confirm the formation of NiRe alloy. Additionally,
193 elemental mapping and line scanning of Ni₁Re₁ were also performed (Figure 2(e, f)). The result of
194 mapping analysis showed that the Ni and Re species were successfully dispersed on the SBA-15 surface.
195 A similar trend of Ni and Re components displayed in the line scanning profile indicated that Ni and Re
196 species existed an interaction.



197
198 **Figure 3.** XPS spectra of (a) Ni 2p and (b) Re 4f for the reduced catalysts.

199 XPS was used to analyze the oxidation state of catalysts and the possible electronic interaction
200 between metals. Figure 3(a) shows the Ni 2p spectra and corresponding divided peaks of each sample.

201 For the monometallic Ni₁ catalyst, the Ni 2p spectra displayed three deconvoluted peaks, locating at
202 852.9, 856.1 and 861.1 eV, which were ascribed to the Ni⁰, Ni²⁺ and its satellite peak [32], respectively.
203 As compared with the Ni₁ catalyst appeared at 852.9 eV for Ni⁰, the binding energy (BE) of Ni⁰ shifted
204 to higher BE (+0.7) in the Ni₁Re₁ catalyst, indicating the electron transfer from the metallic Ni to Re.
205 Figure 3(b) shows the Re 4f spectra of Re₁ and Ni₁Re₁ catalysts. Divided peaks of each sample showed
206 a mixture of different oxidation states (Re⁰, Re²⁺, Re⁷⁺) [21, 33]. As expected, the characteristic peak of
207 Re⁰ in the Ni₁Re₁ catalyst shifted to lower BE (from 40.4 eV in Re₁ catalyst to 40.1 eV) as compared
208 with the monometallic Re₁ catalyst. The increase in BE of metallic Ni and the decrease in BE of metallic
209 Re in the Ni₁Re₁ catalyst suggest that there is an electronic interaction between Ni and Re species.



210
211 **Figure 4.** In situ FTIR of CO adsorption over the reduced catalysts at room temperature for 30 min in a
212 CO flow, and then desorption in N₂ flow for 5, 10, 15, 20, 25 min of (a) Ni₁ and (b) Ni₁Re₁.

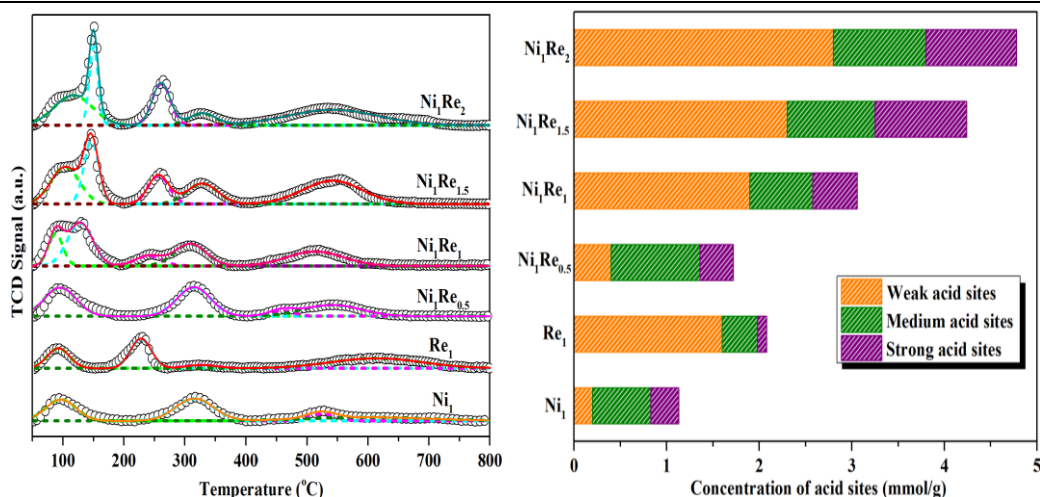
213 In order to further investigate the interaction between Ni and Re species, in situ FT-IR of CO
214 adsorption-desorption on Ni₁ and Ni₁Re₁ catalysts were performed (Figure 4). Typically, the band
215 appeared in below 2000 cm⁻¹ was attributed to the multi-coordinated adsorption of CO, while the band
216 located in above 2000 cm⁻¹ was ascribed to the linear adsorption of CO [34]. It was reported that CO was

217 hardly adsorbed on the Re species (metallic Re and ReO_x) at room temperature [31], therefore, the bands
218 shown in Figure 4 were assigned to the CO adsorption on Ni atoms. From Figure 4((a, b)), it was observed
219 that the Ni_1Re_1 catalyst only showed the bands of linear adsorption of CO, while the Ni_1 catalyst exhibited
220 both multi-coordinated adsorption (1628 cm^{-1}) and linear adsorption of CO. This may be due to the fact
221 that introducing Re breaks the contiguous Ni atoms and forms much small Ni ensembles, which
222 suppressed the multi-coordinated adsorption of CO on Ni atoms.

223 Besides, it was observed that the band of linear CO adsorption showed a blue-shift from 2040 cm^{-1}
224 on Ni_1 to 2053 cm^{-1} on Ni_1Re_1 . Combining the above XPS results, this shift may result from the electronic
225 interaction between Ni and Re species, which the decrease of Ni electron density results in the weakening
226 of Ni-C bonds and strengthening of C-O bonds [31], and thus leading to the blue-shift of $\nu(\text{C}\equiv\text{O})$.
227 Additionally, we can clearly see that, after flushed with flow N_2 for 20 min, Ni_1Re_1 catalyst still exhibited
228 the strong adsorption peaks of CO, while the peaks were not detected on the Ni_1 catalyst. This suggests
229 that Ni_1Re_1 bimetallic catalyst provided more active sites for the CO linear adsorption, and these sites
230 have strong interaction with CO. Carbon monoxide as a simplified model for C=O group, the strong
231 interaction indicates that the reactant molecules containing C=O groups can be better adsorbed on the
232 Ni_1Re_1 bimetallic catalyst.

(a)

(b)



233

234 **Figure 5.** (a) NH₃-TPD profiles of the reduced catalysts; (b) corresponding acid concentration obtained

235 by calculating the fitted peak area.

236 Catalyst acidity plays an important role in promoting the conversion of fatty acids and improving

237 the selectivity of fatty alcohols. Appropriate acid site concentrations are beneficial for the reaction, while

238 the weak and strong acid concentrations usually result in the low catalytic activity and the occurrence of

239 side reactions like C-C bond cleavage, respectively. To study the influence of the introduced Re species

240 on the catalyst acidity, NH₃-TPD characterization was performed. According to the different NH₃

241 desorption temperatures, the acidic sites were divided into three types of weak ($T < 300$ °C), medium

242 (300 °C $< T < 450$ °C) and strong acid sites ($T > 450$ °C) [35]. As shown in Figure 5 (a), all tested catalysts

243 were dominated by weak and medium acid sites. As compared with the monometallic Ni₁ catalyst,

244 introducing Re species greatly increased the number of weak and medium acid sites. This could be

245 attributed to the unsaturated Reⁿ⁺ species, as proved in the XPS characterization. The corresponding acid

246 concentrations were obtained based on the fitted peak area (Figure 5 (b)). With the introduction of Re

247 species, the total acid concentration was gradually increased. However, when excessive Re species were

248 added, it was noted that a large number of strong acid sites were detected on the Ni₁Re_{1.5} and Ni₁Re₂

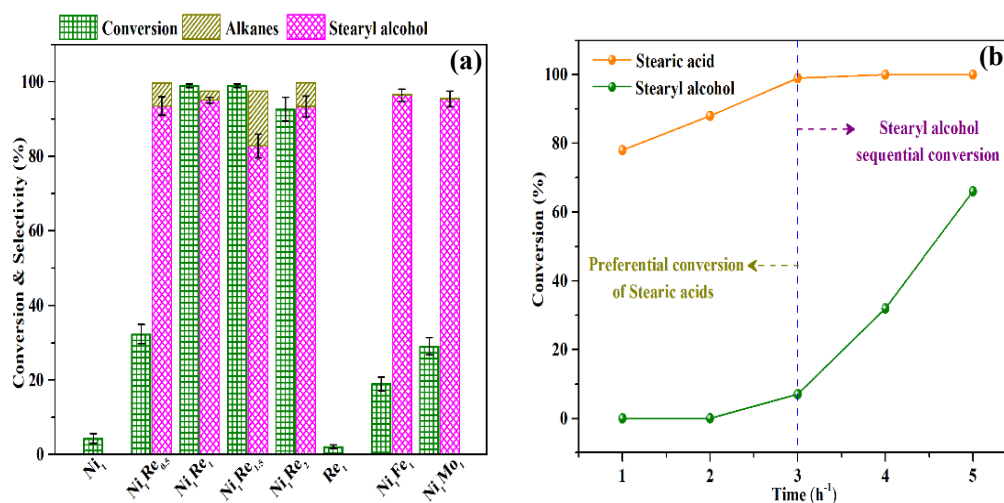
249 catalysts (Figure 5 (a)). Based on the XRD characteristic results, this may be caused by excessive Re

250 species forming large metal particles. These results suggest that the acidity of Ni_xRe_y catalysts mainly
251 result from the introduction of the Re species, however, adding an excessive amount of Re species would
252 result in the appearance of strong acid sites.

253 **3.2 Catalytic performance towards hydrogenation of fatty acids**

254 In order to evaluate the catalytic performance in the hydrogenation of fatty acids, all synthesized
255 catalysts were applied to hydrogenation of stearic acid. As shown in [Figure 6\(a\)](#), at a low temperature of
256 150 °C, monometallic Ni₁ and Re₁ catalysts exhibited low catalytic activities with conversion rates of <
257 10%. In contrast, the Ni_xRe_y bimetallic catalysts with different molar ratio showed remarkably enhanced
258 catalytic performance, where the main products were stearyl alcohol and a small amount of side product
259 of alkanes. The optimum catalytic performance was observed on the Ni₁Re₁ catalyst with 100%
260 conversion and 95% selectivity towards stearyl alcohol. Further increasing Re loading (Ni₁Re₂ catalyst)
261 resulted in the decrease of catalyst activity and selectivity. Decreasing surface area, large Re metal
262 particles and strong acid sites on the Ni₁Re₂ catalysts may be the main reason for the decrease of catalytic
263 performance, as indicated by the above XRD ([Figure 1\(a\)](#)) and NH₃-TPD ([Figure 5](#)) characterizations.
264 On the other hand, it was reported that the FeO_x- [18] and MoO_x-modified [36, 37] metallic Ni catalysts
265 are efficient for hydrogenation of fatty acids/esters. For comparison, their catalytic activities were tested
266 under the selected conditions and found to be ineffective. These results suggest that introducing Re
267 component is essential to realize the low-temperature hydro-conversion of stearic acid. According to the
268 above catalyst characterization, it is known that there is an interaction between Ni and Re species in the
269 bimetallic catalysts, therefore, we infer that the interaction may be responsible for its high catalytic
270 activity. To verify this speculation, a physical mixture of Ni₁ and Re₁ was tested and showed similar
271 stearic acid conversion (6.5%) as the Ni₁ catalyst, indicating the importance of a combination of a

272 proximate Ni and Re species.

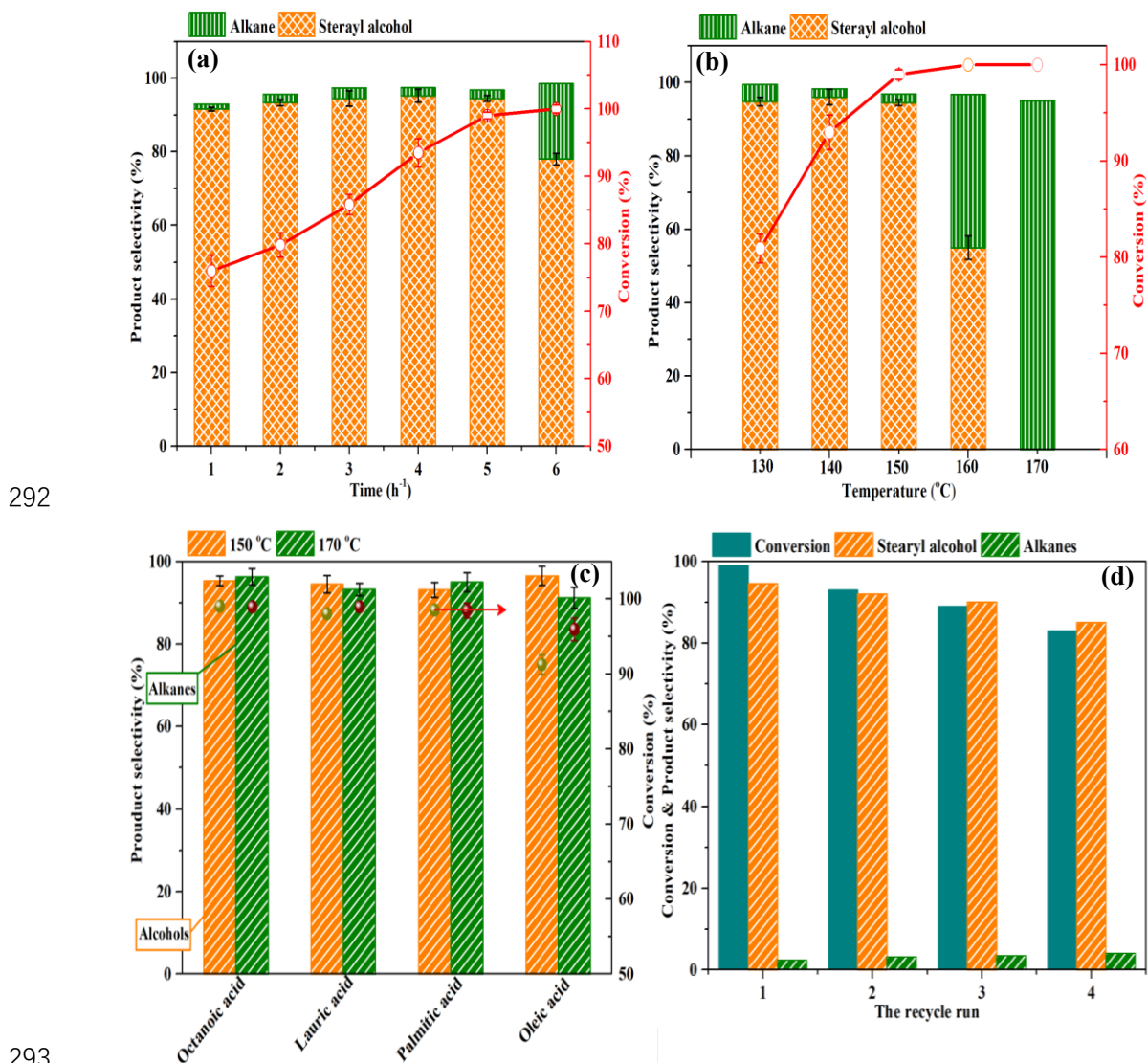


273

274 **Figure 6.** (a) the conversion of stearic acid and product distributions over the different catalysts; (b)
 275 competitive conversion of stearic acid and stearyl alcohol over the Ni₁Re₁ catalyst with reaction time.
 276 Reaction conditions: (a) 0.1 g stearic acid, 0.02 g catalyst in 10 mL cyclohexane at 150 °C and 4.0 MPa
 277 H₂ for 5 h, (b) reactants containing both stearic acid (0.05 g) and stearyl alcohol (0.05 g), other reaction
 278 parameters are the same as (a).

279 Next, we used stearic acid and stearyl alcohol as raw materials to study their conversion process on
 280 the Ni₁Re₁ catalyst (Figure 6(b)). At the beginning of reaction (0~3h), stearic acid was first converted,
 281 while stearyl alcohol was not consumed at the presence of stearic acid. After 3h reaction, stearyl alcohol
 282 begin to be converted when stearic acid was completely consumed. This result suggests that stearic acid
 283 was preferentially adsorbed and converted on the Ni₁Re₁ catalyst than the stearyl alcohol. In other words,
 284 the presence of stearic acid can inhibit the conversion of stearyl alcohol on the Ni₁Re₁ catalyst. This is
 285 consistent with prior study of fatty acid over the ReO_x-Pd/SiO₂ catalyst [38]. The preferential conversion
 286 sequence of fatty acids and fatty alcohols on the Ni₁Re₁ catalyst makes it possible to selectively obtain
 287 fatty alcohols and diesel-range alkanes with high yields by adjusting reaction temperature. This feature
 288 of the Ni₁Re₁ catalyst may be attributed to its strong electrophilicity, as indicated in the CO-FTIR

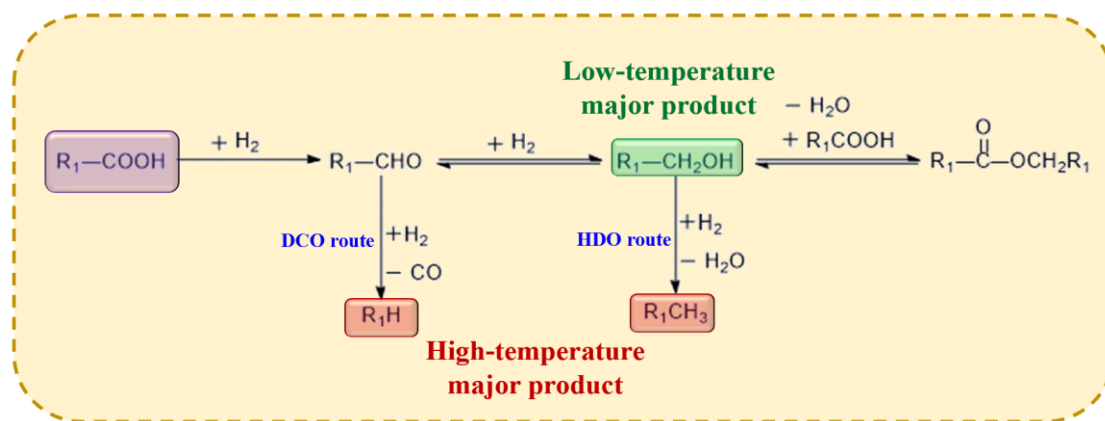
289 characterization (Figure 4). Since the carbonyl oxygen of fatty acids is more electronegative than the
 290 hydroxyl oxygen of fatty alcohols [39], thus, the fatty acids are preferentially adsorbed and converted
 291 on the catalyst surface than the fatty alcohols.



293
 294 **Figure 7.** Catalytic conversion and the main product distributions as function of (a) reaction time, (b)
 295 reaction temperature, (c) hydrogenation of various fatty acids and (d) catalyst recycling test on the Ni₁Re₁
 296 catalyst. General conditions: (a) 0.1 g stearic acid, 0.02 g catalyst (Ni₁Re₁ catalyst) in 10 mL cyclohexane
 297 at 150 °C and 4.0 MPa H₂ for 5 h.

298 Figure 7(a) shows the time-course experiments of stearic acid, and reveals that the reactant was
 299 gradually converted to products with time. In the initial reaction stage of 2 h, the products were stearyl

300 alcohol and a small amount of alkanes and stearyl stearate. After 5 h reaction, the reactant was completely
301 converted and the dominant product was stearyl alcohol. Further prolonging the reaction time (6 h), the
302 obtained fatty alcohol was gradually converted into alkanes containing C₁₇ and C₁₈ alkanes via
303 dehydrogenation-decarbonylation route (DCO route) and dehydration-hydrogenation route (HDO route),
304 respectively, as shown in Scheme 1. The optimum reaction time was 5 h, in which the reactant was
305 completely converted and the selectivity of fatty alcohol was the highest (95%). Figure 7(b) shows the
306 effect of reaction temperature on the conversion and product distributions. This result suggests that, by
307 adjusting reaction temperature, fatty alcohols or alkanes with high yields can be selectively obtained. For
308 instance, fatty alcohols were the main product at a low temperature of 150 °C, while the alkanes were
309 obtained at a higher temperature of 170 °C. In addition, by studying the influence of H₂ pressure on the
310 hydrogenation reaction, it was found that 4.0 MPa H₂ pressure was satisfactory (Figure S2).



311

312

Scheme 2. Possible reaction pathway of fatty acids over the Ni₁Re₁ catalyst.

313

314

315

316

Under the optimized reaction conditions, the scope of substrates was extended to other fatty acids such as octanoic acid, lauric acid, palmitic acid and oleic acid. As shown in Figure 7(c), the Ni₁Re₁ bimetallic catalyst basically achieved quantitative saturated acids (octanoic acid, lauric acid and palmitic acid) conversion and gave their corresponding fatty alcohol as the dominate product. For the unsaturated

317 acid of oleic acid, the relatively low conversion rate (92%) may be attributed to its unsaturated C=C bond,
318 which consumed a large amount of hydrogen molecules in reaction system. Further raising the reaction
319 temperature to 170 °C, the diesel-range alkanes with high yields can be obtained. [Table 1](#) displays the
320 performance of Ni₁Re₁ catalyst and a comparison with previous reported catalyst system during the
321 hydrogenation of fatty acids [[11](#), [16](#), [18](#), [40-44](#)]. The developed Ni₁Re₁ catalyst shows excellent catalytic
322 performance for production of diesel-range alkanes and fatty alcohols from the conversion of fatty acid
323 at low temperature, and even better than noble metal catalysts. In addition, it is highlighted that,
324 compared with the other catalysts, Ni₁Re₁ catalyst exhibits tunable selectivity towards alcohols and
325 alkanes in a low-temperature range of 150 and 170 °C. These results are important not only for the
326 conversion of waste cooking oils rich in fatty acids under mild conditions, but also for the selective
327 hydrogenation of other biomass-derived compounds containing C=O/C-O and O-H groups.

328 Catalyst stability as an important indicator for evaluating heterogeneous catalyst was also studied
329 ([Figure 7\(d\)](#)). After the fourth recycling test, the conversion and selectivity towards stearyl alcohol were
330 decreased by about 15% (from 99% to 84%) and 10% (from 95% to 85%), respectively. TEM, XPS and
331 ICP-MS characterizations were employed to elucidate the decrease of the catalytic performance. TEM
332 images ([Figure S3](#)) showed that the metal nanoparticles after recycling were still evenly dispersed on the
333 catalyst surface, and no obvious agglomeration was observed. The XPS spectra ([Figure S4](#)) revealed that
334 after recycles, the ratio of Ni⁰ decreased from 9.2% to 4.3%, while the Re⁰ decreased from 7% to 3.2%.
335 ICP-MS results ([Table S3](#)) indicated that the contents of Ni (from 6.8 wt% to 6.3 wt%) and Re (from
336 21.8 wt% to 19.2 wt%) species were decreased after recycles. Therefore, the changes of catalyst activity
337 and selectivity may be attributed to the oxidation of partially metal active sites and the leaching of metal
338 elements. The above recycle results indicate that the reusability of the catalyst need to be further

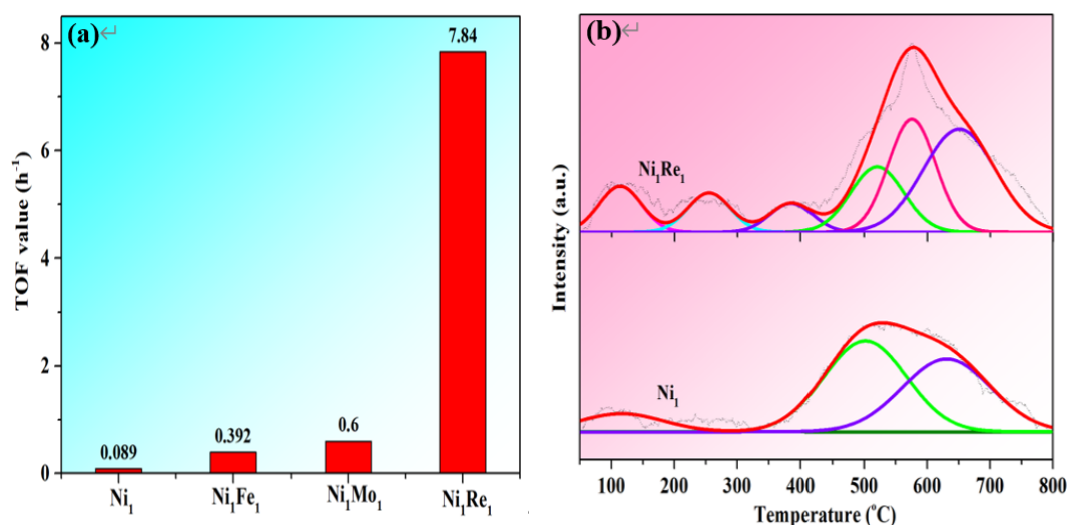
339 improved. In future work, how to inhibit the leaching of metal active species during reactions will be the
 340 focus of our research.

341 **Table 1.** The performance of Ni₁Re₁ in this work and comparison with previous reported studies

Catalyst	Reaction conditions	Solvent	Conv. (%)	Alcohol selec. (%)	Alkane selec. (%)	Ref.
Ru-Sn/SiO ₂	240 °C, 4.0 MPa	dodecane	100	99.0	0.55	40
Ru/NH ₂ -rGO	210 °C, 10.0 MPa	1,4-dioxane	>99	93.0	—	41
Ni-Fe/C	250 °C, 5.0 MPa	1,4-dioxane	>99	98.0	—	18
Ni-In/SiO ₂	270 °C, 3.5 MPa	cyclohexane	100	94.1	—	16
Ni ₁ Re ₁	150 °C, 4.0 MPa	cyclohexane	99	94.5	2.3	This work
Ir-ReO _x /SiO ₂	180 °C, 2.0 MPa	cyclohexane	100	—	100%	11
Ru/HPA	180 °C, 2.0 MPa	H ₂ O	95.8	15	80.7	42
Ni/ZrO ₂	260 °C, 3.0 MPa	dodecane	100	1.2	97.5	43
CuCo/CNT	260 °C, 3.0 MPa	decane	100	—	95.0	44
Ni ₁ Re ₁	170 °C, 4.0 MPa	cyclohexane	100	—	95.0	This work

342 3.3 Studies on structure-activity correlation

343 Normally, bimetallic catalysts had higher catalytic performance due to their unique synergistic
 344 effects as compared with the monometallic catalysts in the HDO reactions. As shown in [Figure 8\(a\)](#),
 345 bimetallic catalysts such as Ni₁Fe₁, Ni₁Mo₁ and Ni₁Re₁ showed higher TOF values than that of
 346 monometallic Ni catalyst under the identical reaction conditions. Among these bimetallic catalysts,
 347 Ni₁Re₁ catalyst exhibited highest TOF value, indicating that the introduction of Re species is crucial to
 348 enhance the catalytic activity. Based on the above characteristic results (XRD, HRTEM, XPS and CO-
 349 FTIR), it was known that the introduced Ni and Re species interacted with each other and were mainly
 350 dispersed on the surface of the catalyst in the form of NiRe alloy. Therefore, we infer that the high
 351 catalytic activity may be associated with the NiRe alloy, that is, promoting the dissociation/activation of
 352 H₂ and the adsorption/conversion of reactants at low temperatures.



353

354 **Figure 8.** (a) Comparison of TOF values over the different reduced catalysts. (b) H₂-TPD profiles of the
355 reduced Ni₁ and Ni₁Re₁ catalysts.

356

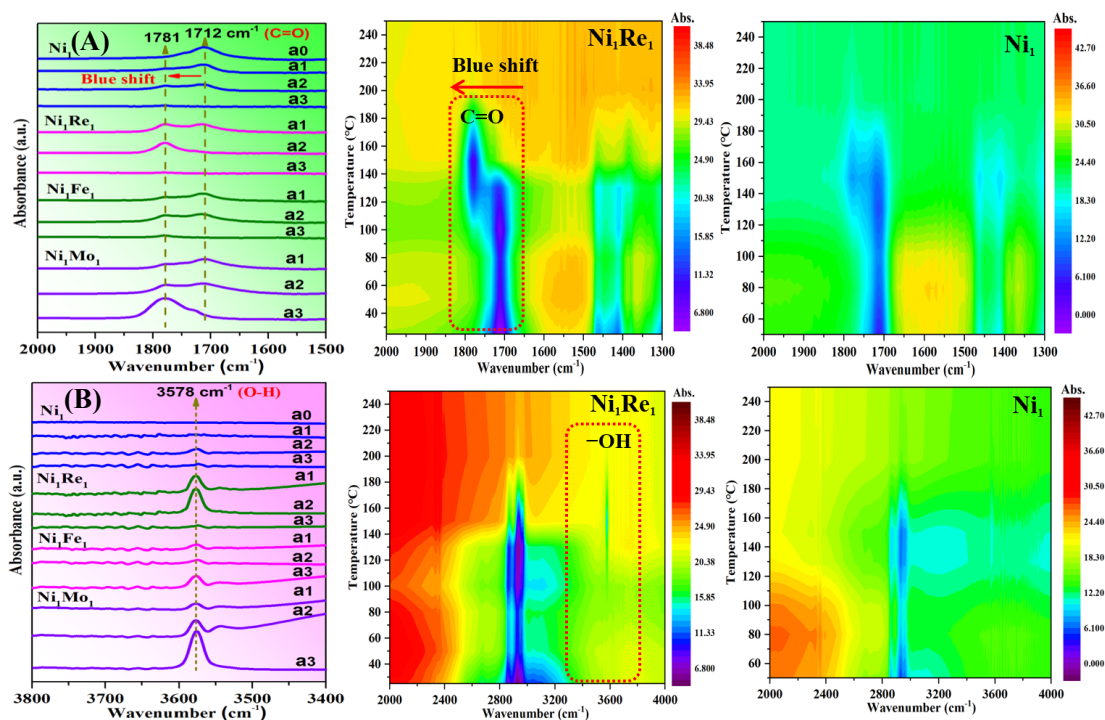
357 In order to investigate the ability of H₂ dissociation/activation on the catalysts, H₂-TPD experiments
358 were performed (Figure 8(b)). Compared with the reference sample of Ni₁ catalyst showing the H₂
359 desorption peaks at high temperatures, several desorption peaks at a low temperature range (100-400 °C)
360 were observed in the Ni₁Re₁ bimetallic catalyst. Moreover, the Ni₁Re₁ bimetallic catalyst showed a larger
361 integral peak area than that of Ni₁ catalyst. These results indicate that introducing Re species can enhance
362 hydrogen activation/dissociation ability, which can provide more active hydrogen atoms for the
363 hydrogenation reaction. This enhanced H₂ activation/dissociation ability on the Ni₁Re₁ catalyst can also
364 be supported by the following DFT calculation (Figure 10).

364

365 To acquire more adsorbed information about the reactant on the catalysts, in situ FTIR of octanoic
366 acid was conducted. As shown in Figure 9(A), a peak at 1720 cm⁻¹ was detected corresponding to the
367 carbonyl group (C=O) of the pure octanoic acid [45, 46]. As the temperature increased from 25 °C to 150
368 °C, the peak gradually shifted to a higher wavenumber (1781 cm⁻¹), indicating that the octanoic acid was
369 chemical adsorbed on the tested catalysts. Compared with the Ni₁ catalyst that showing a weak peak
369 intensity at 1781 cm⁻¹, Ni₁Re₁ catalyst showed a strong peak intensity, especially at 150 °C, where the

370 adsorbed peak at 1721 cm^{-1} was completely shifted to 1781 cm^{-1} . This result demonstrates that, with an
371 increased in reaction temperature, fatty acid molecules can be more stably adsorbed on the Ni_1Re_1 catalyst
372 via interacting with carbonyl group of fatty acids when compared with the Ni_1 catalyst, and this
373 interaction reached the strongest at $150\text{ }^\circ\text{C}$. Furthermore, to study the effect of introducing Re species on
374 the reactant adsorption, in situ FTIR spectrum of the octanoic acid on the NiRe catalysts with various
375 Ni/Re ratios were carried out. As shown in [Figure S5](#), monometallic Re_1 and bimetallic Ni_xRe_y catalysts
376 exhibited a higher adsorption intensity as compared with the Ni_1 catalysts under the identical desorbed
377 temperature, which suggests that the introduction of Re species enhanced the interaction between the
378 reactant and catalyst, in accordance with the DFT calculation results.

379 On the other hand, the adsorbed information about the reactant on the Ni_1Fe_1 and Ni_1Mo_1 catalysts
380 was also investigated for comparison. It was observed that the Ni_1Fe_1 and Ni_1Mo_1 catalysts showed
381 stronger peak intensity at 1781 cm^{-1} under the identical adsorbed temperatures as compared with the Ni_1
382 catalyst. This indicates that introducing the second metal (Fe and Mo) is beneficial to promote the
383 adsorption of fatty acids due to their higher oxophilicity than the metallic Ni. Secondly, analyzing the
384 spectra of the bimetallic catalysts found that the temperatures of Ni_1Re_1 , Ni_1Fe_1 and Ni_1Mo_1 catalysts
385 achieving completely transformation from 1712 to 1781 cm^{-1} were 150 , 200 and $200\text{ }^\circ\text{C}$, respectively.
386 This reveals that, compared with the Ni_1Fe_1 and Ni_1Mo_1 catalysts, Ni_1Re_1 catalyst can chemically adsorb
387 the fatty acids at a lower temperatures ($150\text{ }^\circ\text{C}$) via interacting with carbonyl group.



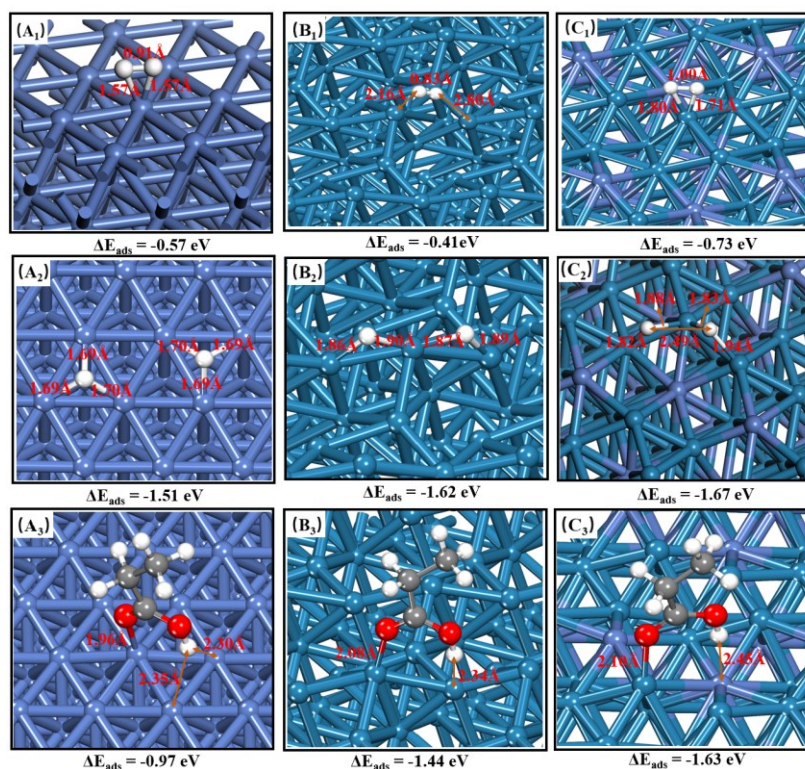
388

389 **Figure 9.** In situ FTIR spectra of octanoic acid at 1500-2000 cm^{-1} (A), 3400-3800 cm^{-1} (B) over the Ni₁,
 390 Ni₁Re₁, Ni₁Fe₁ and Ni₁Mo₁ catalysts: (a0) 25 °C, (a1) 130 °C, (a2) 150 °C, (a3) 200 °C.

391 Another difference in the spectra for these catalysts was the band at 3578 cm^{-1} , which is attributed
 392 to the hydroxy group of fatty alcohol products [42]. As shown in Figure 9(B), Ni₁ catalyst showed a weak
 393 peak intensity, while Ni₁Re₁, Ni₁Fe₁ and Ni₁Mo₁ bimetallic catalysts showed a strong peak intensity. As
 394 the environmental temperature increased, the peak intensity gradually becomes stronger. Moreover, it is
 395 noted that as the peak intensity of the carbonyl group (C=O) of the octanoic acid decreased (Figure 9(A)),
 396 the intensity of the hydroxy group gradually increased, indicating that the octanoic acid are gradually
 397 transformed to octanol as temperature increased. Among these bimetallic catalysts, Ni₁Re₁ and Ni₁Mo₁
 398 catalysts showed higher peak intensity than that of Ni₁Fe₁ catalyst. Compared with the Ni₁Mo₁ catalyst
 399 that showing strong peak intensity at 200 °C, Ni₁Re₁ catalyst exhibited the highest peak intensity at 150
 400 °C. These results proved that Ni₁Re₁ catalyst can adsorb and convert fatty acid molecules into fatty
 401 alcohols at a lower temperature as compared with the Ni₁, Ni₁Fe₁ and Ni₁Mo₁ catalysts, in accordance

402 with the experimental results shown in [Figure 6\(a\)](#).

403 In order to further study the ability of H₂ dissociation/activation and the adsorption behavior of fatty
404 acids on the metallic Ni, Re, and NiRe alloy, DFT calculations are carried out ([Figure 10](#)). The Ni (111),
405 Re (111) and Re₃Ni alloy (111) catalysts were constructed as simplified models for calculations in this
406 work. Here, a more negative adsorption energy value represents a stronger interaction and a more stable
407 adsorption state [39]. For the hydrogenation reaction, it is known that the H₂ dissociation/activation on
408 the surface of catalyst is usually a prerequisite. Therefore, we first studied the ability of H₂
409 dissociation/activation on the above-mentioned catalyst models. As shown in [Figure 10A₁-C₁](#), the Re₃Ni
410 alloy (111) showed a stronger interaction with H₂ molecules as compared with the Ni (111) catalyst
411 (adsorption energies: -0.73 vs -0.57 eV). This strong interaction between the Re₃Ni alloy (111) and H₂
412 molecules greatly promoted the dissociation of H₂ and thus provided more active hydrogen atoms for the
413 hydrogenation reaction, as proved in [Figure 10A₂-C₂](#).



414

415 **Figure 10.** Optimized adsorption structures of H₂ on (A₁) Ni (111), (B₁) Re (111) and (C₁) Re₃Ni alloy
416 (111); of H* on (A₂) Ni (111), (B₂) Re (111) and (C₂) Re₃Ni alloy (111); of PA molecular on (A₃) Ni (111),
417 (B₃) Re (111) and (C₃) Re₃Ni alloy (111). Ni: purple; Re: dark green; O: red (in PA); H: white; C: dark
418 gray.

419 **Figure 10C₁-C₃** shows the adsorption state of propionic acid (PA: a model molecule of fatty acids)
420 on the Ni (111), Re (111) and Re₃Ni alloy (111) models. The above three models reveals that the PA
421 molecule was adsorbed on the surface of catalysts through the interaction with oxygen atom of carbonyl
422 group of fatty acids, in consistent with the characteristic results of **Figure 9A**. The calculated results
423 showed that the adsorption energies over the Ni (111), Re (111) and Re₃Ni alloy (111) were -0.97, -1.44
424 and -1.63 eV, respectively. The Re₃Ni alloy (111) showed the highest negative PA adsorption energy,
425 suggesting that PA could be more stably adsorbed on the surface of Re₃Ni alloy (111) catalyst. These
426 calculation results are in accordance with the above H₂-TPD and in-situ FTIR characterizaiton results. In
427 summary, from the above characterizaiton and DFT calculation results, it can be concluded that the high
428 catalytic performance of NiRe bimetallic catalysts was mainly attributed to its strong ability of H₂
429 dissociation/activation and strong oxophilicity for the adsorption of fatty acids at low temperature.

430 **4. Conclusions**

431 In summary, we reported an efficient and environmentally benign catalytic system for the
432 hydrogenation of fatty acids under remarkably low temperatures over the Ni₁Re₁ catalyst. At 150 °C, a
433 high fatty acids conversion (>95%) and fatty alcohols selectivity (>90%) can be obtained. Further
434 increasing the temperature to 170 °C, the reactant can be completely converted into diesel-range alkanes.
435 Studies on structure-activity correlation indicate that the high catalytic activity was attributed to the
436 formation of NiRe alloy, which improved the dispersion of metallic Ni, the ability of H₂
437 dissociation/activation, and enhanced the adsorption of fatty acids/alcohols. The high selectivity towards

438 target products was ascribed to its strong electrophilicity, making fatty acids preferentially adsorb on the
439 catalyst surface than fatty alcohols, which results in high efficiency and inhibits the conversion of target
440 products during the reaction. These features of the Ni-Re bimetallic catalyst may also enable it applicable
441 to the hydro-conversion of other biomass-derived oxygenates containing C=O/C-O and/or O-H groups
442 into valuable chemicals and green biofuels.

443 **Acknowledgements**

444 The authors would like to thank the financial support provided by the National Natural Science
445 Foundation of China (2019YFB1504005 and 2019YFB1504000).

446 **References**

- 447 [1] L. Hermida, A.Z. Abdullah, A.R. Mohamed. Deoxygenation of fatty acid to produce diesel-like
448 hydrocarbons: a review of process conditions, reaction kinetics and mechanism. *Renewable and*
449 *Sustainable Energy Reviews*. 42 (2015) 1223-1233.
- 450 [2] X. Yao, T.J. Strathmann, Y. Li, L.E. Cronmiller, H. Ma, J. Zhang. Catalytic hydrothermal
451 deoxygenation of lipids and fatty acids to diesel-like hydrocarbons: a review. *Green Chemistry*. 23
452 (2021) 1114-1129.
- 453 [3] Y. Zhou, X. Liu, P. Yu, C. Hu. Temperature-tuned selectivity to alkanes or alcohol from ethyl
454 palmitate deoxygenation over zirconia-supported cobalt catalyst. *Fuel*. 278 (2020) 1-13.
- 455 [4] J. Pritchard, G.A. Filonenko, R. van Putten, E.J.M. Hensen, E.A. Pidko. Heterogeneous and
456 homogeneous catalysis for the hydrogenation of carboxylic acid derivatives: history, advances and
457 future directions. *Chemical Society Review*. 44 (2015) 3808-3833.
- 458 [5] Z.H. Zhang, Q.W. Yang, H. Chen, K. Chen, X.Y. Lu, P.K. Ouyang, J. Fu, J.G. Chen. In situ
459 hydrogenation and decarboxylation of oleic acid into heptadecane over a Cu-Ni alloy catalyst using

- 460 methanol as a hydrogen carrier. *Green Chemistry*. 20 (2018) 197-205.
- 461 [6] S. Brillouet, E. Baltag, S. Brunet, F. Richard. Deoxygenation of decanoic acid and its main
462 intermediates over unpromoted and promoted sulfided catalysts. *Applied Catalysis B: Environmental*
463 148 (2014) 201-211.
- 464 [7] S.K. Kim, S. Brand, H.-S. Lee, Y. Kim, J. Kim. Production of renewable diesel by hydrotreatment of
465 soybean oil: effect of reaction parameters. *Chemical Engineering Journal*. 228 (2013) 114-123.
- 466 [8] H. Adkins, K. Folkers. The catalytic hydrogenation of esters to alcohols. *Journal of the American*
467 *Chemical Society*. 53 (1931) 1095-1097.
- 468 [9] T. Turek, D.L. Trimm, N.W. Cant. The catalytic hydrogenolysis of esters to alcohols. *Catalysis*
469 *Review*. 36 (1994) 645-683.
- 470 [10] Y.D. Zhou, L. Li, G.Y. Li, C.W. Hu. Insights into the influence of ZrO₂ crystal structures on methyl
471 laurate hydrogenation over Co/ZrO₂ catalysts. *ACS Catalysis*. 11 (2021) 7099-7113.
- 472 [11] S. Liu, T. Simonetti, W. Zheng, B. Saha. Selective hydrodeoxygenation of vegetable oils and waste
473 cooking oils to green diesel using a silica-supported Ir-ReO_x bimetallic catalyst. *ChemSusChem*. 11
474 (2018) 1446-1454.
- 475 [12] A. Ali, B. Li, Y. Lu, C. Zhao. Highly selective and low-temperature hydrothermal conversion of
476 natural oils to fatty alcohols. *Green Chemistry*. 21 (2019) 3059-3064.
- 477 [13] H.G. Manyar, C. Paun, R. Pilus, D.W. Rooney, J.M. Thompson, C. Hardacre. Highly selective and
478 efficient hydrogenation of carboxylic acids to alcohols using titania supported Pt catalysts. *Chemical*
479 *Communication*. 46 (2010) 6279-6281.
- 480 [14] Z.Y. Pan, R.J. Wang, J.X. Chen. Deoxygenation of methyl laurate as a model compound on Ni-Zn
481 alloy and intermetallic compound catalysts: geometric and electronic effects of oxophilic Zn. *Applied*

- 482 Catalysis B: Environmental. 224 (2018) 88-100.
- 483 [15] Y. Zheng, N. Zhao, J.X. Chen. Enhanced direct deoxygenation of anisole to benzene on SiO₂-
484 supported Ni-Ga alloy and intermetallic compound. Applied Catalysis B: Environmental. 250 (2019)
485 280-291.
- 486 [16] L. Wang, X. Niu, J. Chen. SiO₂ supported Ni-In intermetallic compounds: efficient for selective
487 hydrogenation of fatty acid methyl esters to fatty alcohols. Applied Catalysis B: Environmental. 278
488 (2020) 1-14.
- 489 [17] Z.H. Zhang, H. Chen, C.X. Wang, K.Q. Chen, X.Y. Lu, P.K. Ouyang, J.X. Chen. Efficient and
490 stable Cu-Ni/ZrO₂ catalysts for in situ hydrogenation and deoxygenation of oleic acid into
491 heptadecane using methanol as a hydrogen donor. Fuel. 230 (2018) 211-217.
- 492 [18] X. Kong, Z. Fang, X. Bao, Z. Wang, S. Mao, Y. Wang. Efficient hydrogenation of stearic acid over
493 carbon coated Ni-Fe catalyst. Journal of Catalysis. 367 (2018) 139-149.
- 494 [19] S. Liu, W. Zheng, J. Fu, K. Alexopoulos, B. Saha, D.G. Vlachos. Molybdenum oxide-modified
495 iridium catalysts for selective production of renewable oils for jet and diesel fuels and lubricants.
496 ACS Catalysis. 9 (2019) 7679-7689.
- 497 [20] S. Liu, S. Dutta, W. Zheng, N.S. Gould, Z. Cheng, B. Xu, B. Saha, D.G. Vlachos. Catalytic
498 hydrodeoxygenation of highcarbon furylmethanes to renewable jet-fuel ranged alkanes over a
499 rhenium-modified iridium catalyst. ChemSusChem. 10 (2017) 3225-3234.
- 500 [21] Y. Takeda, T. Shoji, H. Watanabe, M. Tamura, Y. Nakagawa, K. Okumura, K. Tomishige. Selective
501 hydrogenation of lactic acid to 1,2-propanediol over highly active ruthenium-molybdenum oxide
502 catalysts. ChemSusChem. 8 (2015) 1170-1178.
- 503 [22] K.H. Kang, U.G. Hong, Y. Bang, J.H. Choi, J.K. Kim, J.K. Lee, S.J. Han, I.K. Song. Hydrogenation

- 504 of succinic acid to 1,4-butanediol over Re-Ru bimetallic catalysts supported on mesoporous carbon.
505 *Applied Catalysis A: General*. 490 (2015) 153-162.
- 506 [23] Y. Takeda, M. Tamura, Y. Nakagawa, K. Okumura, K. Tomishige. Characterization of Re-Pd/SiO₂
507 catalysts for hydrogenation of stearic acid. *ACS Catalysis*. 5 (2015) 7034-7047.
- 508 [24] M. Jahandar Lashaki, A. Sayari. CO₂ capture using triamine-grafted SBA-15: the impact of the
509 support pore structure. *Chemical Engineering Journal*. 334 (2018) 1260-1269.
- 510 [25] T.L.R. Hewan, A.G.F. Souza, K.T.C. Roseno, P.F. Moreira, R. Bonfim, R.M.B. Alves, M. Schmal.
511 Influence of acid sites on the hydrodeoxygenation of anisole with metal supported on SBA-15 and
512 SAPO-11. *Renewable Energy*. 119 (2018) 615-624.
- 513 [26] P. Gaudin, L. Michelin, L. Josien, H. Nouali, S. Dorge, J.F. Brilhac, E. Fiani, M. Vierling, M.
514 Moliere, J. Patarin. Highly dispersed copper species supported on SBA-15 mesoporous materials
515 for SO_x removal: influence of the CuO loading and of the support. *Fuel Processing Technology*. 148
516 (2016) 1-11.
- 517 [27] G. Kresse, J. Hafner. Ab initio molecular dynamics for liquid metals. *Physical Review B: Condensed
518 Matter and Materials Physics*. 48 (1993) 13115-13118.
- 519 [28] G. Henkelman, B.P. Uberuaga, H. Jónsson, A climbing image nudged elastic band method for
520 finding saddle points and minimum energy paths. *Journal of Chemical Physics*. 113 (2000) 9901-
521 9904.
- 522 [29] F. Yang, N.J. Libretto, M.R. Komarneni, W. Zhou, J.T. Miller, X. Zhu, D.E. Resasco. Enhancement
523 of m-cresol hydrodeoxygenation selectivity on Ni catalysts by surface decoration of MoO_x species.
524 *ACS Catalysis*. 9 (2019) 7791-7800.
- 525 [30] J. Pritchard, A. Ciftci, M.W.G.M. Verhoeven, E.J.M. Hensen, E.A. Pidko. Supported Pt-Re catalysts

- 526 for the selective hydrogenation of methyl and ethyl esters to alcohols. *Catalysis Today*. 279 (2017)
- 527 10-18.
- 528 [31] F. Yang, D. Liu, H. Wang, X. Liu, J. Han, Q. Ge, X.L. Zhu. Geometric and electronic effects of
- 529 bimetallic Ni-Re catalysts for selective deoxygenation of m-cresol to toluene. *Journal of Catalysis*.
- 530 349 (2017) 84-97.
- 531 [32] S. Engels, J. Eick, W. Morke, U. Maier, I. Boszormenyi, K. Matusek, Z. Schay, L. Guzzi.
- 532 Characterization and catalytic activity of unsupported nickel-rhenium catalysts modified by calcium
- 533 oxide. *Journal Catalysis*. 103 (1987) 105-114.
- 534 [33] K. Liu, J. Pritchard, L. Lu, R. van Putten, M. Tiny Verhoeven, M. Schmitkamp, X.M. Huang, L.
- 535 Lefort, C.J. Kiely, E.G.M. Hensen, E.A. Pidko. Supported nickel-rhenium catalysts for selective
- 536 hydrogenation of methyl esters to alcohols. *Chemical Communications*. 53 (2017) 9761-9764.
- 537 [34] J. Yu, Y. Yang, L. Chen, Z. Li, W. Liu, E. Xu, Y.J. Zhang, S. Hong, X. Zhang, M. Wei. NiBi
- 538 intermetallic compounds catalyst toward selective hydrogenation of unsaturated aldehydes. *Applied*
- 539 *Catalysis B: Environmental*. 277 (2020) 1-9.
- 540 [35] E. Kordouli, B. Pawelec, K. Bourikas, C. Kordulis, J.L.G. Fierro, A. Lycourghiotis. Mo promoted
- 541 Ni-Al₂O₃ co-precipitated catalysts for green diesel production. *Applied Catalysis B: Environmental*.
- 542 229 (2018) 139-154.
- 543 [36] X.C. Cao, F. Long, Q.L. Zhai, P. Liu, J.M. Xu, J.C. Jiang. Enhancement of fatty acids
- 544 hydrodeoxygenation selectivity to diesel-range alkanes over the supported Ni-MoO_x catalyst and
- 545 elucidation of the active phase. *Renewable Energy*. 162 (2020) 2113-2125.
- 546 [37] P. Kumar, S.K. Maity, D. Shee. Role of NiMo alloy and Ni species in the performance of
- 547 NiMo/alumina catalysts for hydrodeoxygenation of stearic acid: a kinetic study. *ACS omega*. 4 (2019)

- 548 2833-2843.
- 549 [38] Y. Takeda, Y. Nakagawa, K. Tomishige. Selective hydrogenation of higher saturated carboxylic
- 550 acids to alcohols using a $\text{ReO}_x\text{-Pd/SiO}_2$ catalyst. *Catalysis Science & Technology*. 2 (2012) 2221-
- 551 2223.
- 552 [39] S.Y. Xing, Y. Liu, X.C. Liu, M. Li, J.Y. Fu, P.F. Liu, P.M. Lv, Z.M. Wang. Solvent-free
- 553 hydrodeoxygenation of bio-lipids into renewable alkanes over NiW bimetallic catalyst under mild
- 554 conditions. *Applied Catalysis B: Environmental*. 269 (2020) 1-11.
- 555 [40] Z. Luo, Q. Bing, J. Kong, J.Y. Liu, C. Zhao. Mechanism of supported Ru_3Sn_7 nanocluster-catalyzed
- 556 selective hydrogenation of coconut oil to fatty alcohols. *Catalysis Science & Technology*. 8 (2018)
- 557 1322-1332.
- 558 [41] L.M. Martínez-Prieto, M. Puche, C. Cerezo-Navarrete, B. Chaudret. Uniform Ru nanoparticles on
- 559 N-doped graphene for selective hydrogenation of fatty acids to alcohols. *Journal of Catalysis*. 377
- 560 (2019) 429-437.
- 561 [42] G. Xu, Y. Zhang, Y. Fu, Q. Guo. Efficient hydrogenation of various renewable oils over Ru-HAP
- 562 catalyst in water. *ACS Catalysis*. 7 (2017) 1158-1169.
- 563 [43] J. Ni, W.H. Leng, J. Mao, J.G. Wang, J.Y. Lin, D.H. Jiang, X.N. Li. Tuning electron density of
- 564 metal nickel by support defects in Ni/ZrO₂ for selective hydrogenation of fatty acids to alkanes and
- 565 alcohols. *Applied Catalysis B: Environmental*. 253 (2019) 170-178.
- 566 [44] J.M. Liang, Z.Y. Zhang, K.J. Wu, Y.C. Shi, W.H. Pu, M.D. Yang, Y.L. Wu. Improved conversion
- 567 of stearic acid to diesel-like hydrocarbons by carbon nanotubes-supported CuCo catalysts. *Fuel*
- 568 *Processing Technology*. 188 (2019) 153-163.
- 569 [45] P.J. Wang, Y. Jing, Y. Guo, Y. Cui, S. Dai, X.H. Y.Q. Liu, Y.Q. Wang. Highly efficient alloyed

- 570 NiCu/Nb₂O₅ catalyst for the hydrodeoxygenation of biofuel precursors into liquid alkanes. *Catalysis*
- 571 *Science & Technology*. 10 (2020) 4256-4263.
- 572 [46] N. Chen, Y. Ren, E.W. Qian. Elucidation of the active phase in PtSn/SAPO-11 for
- 573 hydrodeoxygenation of methyl palmitate. *Journal of Catalysis*. 334 (2016) 79-88.
- 574